Biomaterials 163 (2018) 185–197

Contents lists available at ScienceDirect

Biomaterials

journal homepage: www.elsevier.com/locate/biomaterials

3D-3-culture: A tool to unveil macrophage plasticity in the tumour microenvironment

Sofia P. Rebelo [a, b, 1], Catarina Pinto [a, b, 1], Tatiana R. Martins [a, b], Nathalie Harrer [c], Marta F. Estrada [a, b], Pablo Loza-Alvarez [d], José Cabeçadas [e], Paula M. Alves [a, b], Emilio J. Gualda [d], Wolfgang Sommergruber [c], Catarina Brito [a, b, *]

[a] iBET, Instituto de Biologia Experimental e Tecnológica, Apartado 12, 2780-901, Oeiras, Portugal
[b] Instituto de Tecnologia Química e Biológica António Xavier, Universidade Nova de Lisboa, Av. da República, 2780-157, Oeiras, Portugal
[c] Boehringer Ingelheim RCV GmbH & Co KG, Department of Lead Discovery, 1121, Vienna, Austria
[d] ICFO - Institut de Ciències Fotòniques, The Barcelona Institute of Science and Technology, 08860, Castelldefels, Barcelona, Spain
[e] Serviço de Anatomia Patológica, Instituto Português de Oncologia de Lisboa Francisco Gentil, Lisboa, Portugal

ARTICLE INFO

Article history:
Received 14 December 2017
Received in revised form
9 February 2018
Accepted 12 February 2018
Available online 13 February 2018

Keywords:
3D cancer cell models
Co-culture
Tumour-associated macrophages
Tumour microenvironment
Immunotherapy
Alginate microencapsulation

ABSTRACT

The tumour microenvironment (TME) shapes disease progression and influences therapeutic response. Most aggressive solid tumours have high levels of myeloid cell infiltration, namely tumour associated macrophages (TAM). Recapitulation of the interaction between the different cellular players of the TME, along with the extracellular matrix (ECM), is critical for understanding the mechanisms underlying disease progression. This particularly holds true for prediction of therapeutic response(s) to standard therapies and interrogation of efficacy of TME-targeting agents. In this work, we explored a culture platform based on alginate microencapsulation and stirred culture systems to develop the 3D-3-culture, which entails the co-culture of tumour cell spheroids of non-small cell lung carcinoma (NSCLC), cancer associated fibroblasts (CAF) and monocytes. We demonstrate that the 3D-3-culture recreates an invasive and immunosuppressive TME, with accumulation of cytokines/chemokines (IL4, IL10, IL13, CCL22, CCL24, CXCL1), ECM elements (collagen type I, IV and fibronectin) and matrix metalloproteinases (MMP1/9), supporting cell migration and promoting cell-cell interactions within the alginate microcapsules. Importantly, we show that both the monocytic cell line THP-1 and peripheral blood-derived monocytes infiltrate the tumour tissue and transpolarize into an M2-like macrophage phenotype expressing CD68, CD163 and CD206, resembling the TAM phenotype in NSCLC. The 3D-3-culture was challenged with chemo- and immunotherapeutic agents and the response to therapy was assessed in each cellular component. Specifically, the macrophage phenotype was modulated upon treatment with the CSF1R inhibitor BLZ945, resulting in a decrease of the M2-like macrophages. In conclusion, the crosstalk between the ECM and tumour, stromal and immune cells in microencapsulated 3D-3-culture promotes the activation of monocytes into TAM, mimicking aggressive tumour stages. The 3D-3-culture constitutes a novel tool to study tumour-immune interaction and macrophage plasticity in response to external stimuli, such as chemotherapeutic and immunomodulatory drugs.

1. Introduction

Cell-cell and cell-matrix interactions, involving tumour, stromal and immune cells, are critical in all steps of tumour development and have been extensively studied in recent years. Moreover, reports on their impact on patient prognosis and therapeutic response are also increasing [1,2]. Immune checkpoint blockade and adoptive T-cell therapy approaches have introduced immunotherapies as viable clinical modalities, alongside chemotherapeutics and targeted agents [3]. However, there are still considerable challenges in understanding why in some tumour types immunotherapy has no clinical effect and why certain patients fail to respond to the treatment [4–6]. Undeniably, there is a need to understand the mechanistic effects of a therapy within the immune regulatory context of a given tumour microenvironment

* Corresponding author. Instituto de Tecnologia Química e Biológica António Xavier, Universidade Nova de Lisboa, Av. da República, 2780-157, Oeiras, Portugal.
E-mail address: anabrito@ibet.pt (C. Brito).
[1] The authors contributed equally to the work.

https://doi.org/10.1016/j.biomaterials.2018.02.030

(TME), leading to more effective approaches, and harnessing the full potential of the TME as a therapeutic target [7].

Non-small cell lung cancer (NSCLC), one of the most lethal malignant diseases, is typically associated with extensive myeloid cell infiltration [8,9]. Infiltrating myeloid cells are key mediators of immune suppression, neovascularization, invasiveness, metastasis and poor response to therapy. Consequently, those cells constitute an important target for the development of novel immunotherapies [10,11]. In most solid tumours, including NSCLC, macrophages constitute the main myeloid infiltrate, representing up to 50% of the tumour mass [12,13]. Circulating monocytes are recruited to the tumour tissue and can be transpolarized towards the M1-like or M2-like phenotype. Tumour associated macrophages (TAM) have been linked with the M2-like phenotype, exerting tumour-promoting effects such as induction of proliferation, angiogenesis, ECM remodelling and evasion from adaptive immunity such as secretion of arginase 1 [88]. In contrast, M1 macrophages have a tumour suppressive effect [13]. The presence of TAM infiltrate affects tumour response to standard-of-care drug treatments [14] and were shown to be an important therapeutic target. For instance, by inhibiting the colony stimulating factor 1 receptor (CSF-1R), which is the main route of activation and survival of monocytes, the tumour progression both in murine models as well as in patients was controlled, resulting in an extended survival rate [15–17].

Most of the knowledge on TAM infiltrate has been derived from histological examination of patient samples in retrospective cohort studies where myeloid cells have been identified by a few immunohistochemistry markers, providing no information about the TAM function *per se* [10,18]. Therefore, technological developments are urgently needed including the development of *in vitro* models that can recapitulate tumour-immune interactions in a TME relevant context, while allowing rapid and thorough characterization of the immune compartment, to screen and functionally assess novel therapeutics in high throughput platforms [5].

Preclinical models consist mainly of human tumour-derived cell lines, propagated in 2D culture or used in the implementation of mouse xenografts, and on genetically engineered mouse models (GEMM) of human tumorigenesis [19]. Although 2D cultures provided important insights into potential anticancer agents at early stages of drug development, they cannot recapitulate the gradients of nutrients, oxygen and drug penetration occurring *in vivo* and do not account for key TME triggers [20,21]. Human cell line-derived xenografts differ considerably from primary human tumours in terms of proliferative capacity and TME [22,23]. In addition, the immune system is often compromised, thus these models cannot reliable support immunomodulatory drug development [22]. Immune-competent GEMM overcome some of the drawbacks, as they allow for the presence of the complete immune system. However, those models are still based on murine stromal and immune components [22,24]. For most aggressive cancers, including several lung cancers, drug candidates arising from 2D cell-line screens and mouse xenograft models present poor clinical translation [20]. The discrepancy between these models and the human situation in key physiological features, such as human tumour-stroma, tumour-immune cell interactions and gradients of drug penetration in the tissue have a significant impact on the therapeutic response [20]. Therefore, the combination of *in vivo* cell models with advanced *in vitro* cell models offers a complementary approach to study the mechanisms underlying tumour development in the context of the TME.

3D cellular models have the potential to advance drug discovery and streamline progression of novel candidates through drug discovery pipelines. The need for more predictive drug assays triggered advances in cell culture techniques that led to the appearance of complex *in vitro* models [21]. Tumour spheroids offer an alternative to high throughput monolayer-based assays and are complementary to mouse models [19]. Several methods for spheroid production are currently available, such as low adhesion plates, the hanging drop method, cell-seeded matrices and scaffolds, micropatterning and agitation based methods [25]. Tumour spheroids can mimic drug response of primary human tumours and have proven useful in the study of tumour physiology, such as metabolic and chemical gradients, hypoxic environment and cell-cell and cell-matrix interactions [19,21,26,27]. Heterotypic cellular models have been successfully employed in unravelling new aspects of cancer biology [23,25]. Most heterotypic models include stromal cells, such as cancer-associated fibroblasts (CAF), which have been shown to enhance the inflammatory environment, promote tumour progression and lead to drug resistance [28]. Reports of *in vitro* models of immune interaction with tumours from diverse pathologies are mostly focused on the tumour phenotype and its modulation by the macrophages via secreted factors [29–32]. In lung cancer, it has been reported that the presence of macrophages promotes a metastatic phenotype due to the presence of MMP-1 and VEGF [33]. However, the dynamic interaction between both cell types and the effect of TME heterogeneity on the response to chemotherapeutic or immune-targeted agents has scarcely been assessed in these types of models. Most studies focusing on macrophage and tumour interaction in response to therapy still rely on mouse models using *in vivo* imaging tools that, although capable deciphering tumour architecture and cell interaction networks, are technically demanding and not compatible with high throughput screening [18,34].

In the present work, we established a 3D cell model (3D-3-culture), enclosing three cellular components: NSCLC cells as tumour spheroids, CAF and monocytes. The model is based on the alginate microencapsulation strategy previously described by our group, which allows direct interaction between different cell types and is compatible with continuous monitoring and functional assessment in long-term culture using stirred systems [25,28]. Here we demonstrate the recruitment of human monocytes into tumour tissue and their polarization into a M2-like phenotype without directed differentiation by the addition of exogenous cytokines, thus recreating the TAM phenotype *in vitro*. Moreover, the TME response to therapy is assessed, depicting the differences in each cellular compartment upon treatment and demonstrating that the macrophage phenotype can be modulated in response to chemo- and immunotherapy.

2. Material and methods

2.1. Cell lines

The NSCLC cell line NCI-H157 originally obtained from ATTC (ATCC: #CRL-5802) was stably transfected with the pRSF91. dtTomato-Blasti plasmid [35]. Briefly, 1×10^6 NCI-H157 cells were centrifuged at $90 \times g$ (1200 rpm, 7min.) at room temperature (RT), resuspended in 100 μl Amaxa nucleofector solution, 2 μg of vector DNA were added and carefully mixed. The cell suspension was transferred into an Amaxa cuvette and the cells transfected according to the manufacturer's program (Amaxa Nucleofector™ nuclear transfection apparatus - Lonza; Amaxa Kit Program: V X-0011). After the electroporation procedure, 500 μl of a pre-warmed culture medium containing serum and supplements were added. Culture medium composition was: RPMI media with 11 mM glucose and 2 mM Glutamax (Life Technologies) supplemented with 10% (v/v) FBS (Life Technologies), 1% (v/v) penicillin/streptomycin (Life Technologies), 12 mM HEPES (Life technologies), 1 mM Sodium Pyruvate (Life Technologies) and 0.1 mM of non-essential

amino acids (Life Technologies). The cell suspension was then transferred into a 6-well cell culture plate and an additional 1 ml of the pre-warmed complete medium was added per well. Cells were incubated in a humidified incubator at 37 °C and 5% CO2. Selection was at 30 μg/ml Blasticidin.

Lung derived CAF were isolated as described previously [36]. The local ethics committee "Ethik-Kommission der Medizinischen Fakultät am Universitätsklinikum Tübingen" approved the study (project number 396/2005V and 159/2011BO2) and a written informed consent was obtained from the patient. CAF were immortalized using a virus co-expressing hTERT and GFP (Lenti-hTERT-eGFP; Cat No- LG508, BioGenova), as described [37–39]. CAF were cultivated in RPMI media with 11 mM glucose and 2 mM Glutamax supplemented with 10% (v/v) FBS and 1% (v/v) penicillin/streptomycin (all from Life Technologies).

THP-1 cell line was purchased from ATCC (ATCC: TIB-202) cultured in RPMI media with 11 mM glucose and 2 mM Glutamax supplemented with 10% (v/v) FBS and 1% (v/v) penicillin/streptomycin (all from Life Technologies). For monitoring during the co-culture experiments, the THP-1 cell line was labelled with the fluorescent dye Cell tracker™ deep red (Invitrogen), according to manufacturer's instructions.

Tagged cell lines were used to monitor the different cell lines in co-culture. For fluorescent-based assays/analysis, cultures were performed with non-tagged cell lines. All the cultures were maintained at 37 °C in a humidified atmosphere of 5% CO2 and were sub–cultured every 3–4 days.

2.2. Peripheral blood-derived monocytes (PBM)

Peripheral blood mononuclear cells (PBMC) were isolated from buffy coats obtained from Portuguese Blood Institute. The buffy coats were diluted in phosphate buffer saline (PBS) containing 2% (v/v) FBS and 2 mM EDTA, layered on top of Lymphoprep™ (Stemcell Technologies) and centrifuged at 950 × *g* for 25 min. The PBMC were recovered from the interface and were washed with PBS containing 2% (v/v) FBS and 2 mM EDTA. Monocytes were isolated from PBMC by negative selection through magnetic separation using EasySep™ human monocyte isolation kit (Cat. #19359, Stemcell technologies) and cultured in RPMI media with 11 mM glucose and 2 mM Glutamax supplemented with 10% (v/v) FBS and 1% (v/v) penicillin/streptomycin (Basal Media). Primary monocytes monolayer cultures were maintained in basal media.

2.3. Microencapsulated cultures

NCI-H157 cell line was inoculated as a single cell suspension into 125 ml stirred-tank spinner vessels with flat centered cap and angled side arms (Corning) at a concentration of 3×10^5 cells/mL with an agitation range of 80–100 rpm to induce aggregation.

After 3 days, the spheroids were collected, centrifuged at low speed and combined with single cells of CAF and THP-1/PBM in a ratio of 1:1:1. The spheroid and single cell mix was encapsulated in 1.1% (w/v) of Ultra Pure Ca^{2+} MVG alginate (UP MVG NovaMatrix, Pronova Biomedical), prepared in NaCl 0.9% (w/v) solution. The control groups were the combination of the cellular components (double co-cultures) at a ratio of 1:1 or alone (mono-culture). The microencapsulation was performed in an electrostatically driven unit, VarV1 (Nisco, Zurich, Switzerland) to generate beads with a diameter ranging from 600 to 700 μm. Alginate polymerization was attained with a solution of 20 mM $BaCl_2$ in 115 mM NaCl/5 mM L-Histidine pH 7.4. The microcapsules were collected, washed in NaCl 0.9% (w/v) and cultured in RPMI media with 11 mM glucose and 2 mM Glutamax supplemented with 10% (v/v) FBS and 1% (v/v) penicillin/streptomycin at a concentration of $1–3 \times 10^5$ cells/mL. Cultures were maintained until day 21 when using the THP-1 cell line and until day 10 when using the PBM in stirred conditions and 50% media exchange was performed at each 3–4 days. Samples were collected periodically for determination of culture viability, cell concentration and culture characterization [25,28].

2.4. Spheroid and capsule size

Capsule size was determined by measuring Ferret's diameter and the average tumour spheroid diameter was determined by the average of three diameters per spheroid, using the open source ImageJ software version 1.47 m (http://rsbweb.nih.gov/ij/) [25,28].

2.5. Drug studies

For the 3D-3-culture set up with the THP-1 cell line, the cultures were incubated with drugs 8 days after microencapsulation (day 11 of culture) at a concentration of 25 capsules/mL. Dose-response curves were performed, and cultures were incubated with established concentrations of Paclitaxel (1×10^{-8} M), Cisplatin (1×10^{-6} M) and Blz945 (1×10^{-7} and 1×10^{-6} M). Drug incubation lasted 6 days, with media replenishment. For the 3D-3-culture set up with PBM, the cultures were incubated with BLZ945 4 days after microencapsulation (day 7 of culture) and the drug treatment lasted 3 days. After the drug treatment, metabolic activity, cell proliferation and apoptosis were assessed as described below. For BLZ945 treatment, the macrophage phenotype was characterized by analysis of gene expression and immunodetection of cell surface markers.

2.6. Cell viability

Cell viability was assessed through a fluorescent membrane integrity assay to discriminate live from dead cells. Microcapsules were incubated with 10 μg/mL of fluorescein diacetate (FDA; Sigma-Aldrich) and 1 μM of TO-PRO® 3 (Invitrogen) and were observed under a fluorescence microscope (DMRB6000, Leica). Cells that accumulated the metabolized product of FDA were considered live and cells stained with TO-PRO® 3 were considered dead.

2.7. Apoptosis levels

Apoptosis levels in cultures after exposure to a drug were measured by NucView Apoptosis Assay (Cat. #30062, Biotium). Treated and non-treated cultures were incubated with the caspase 3 substrate Nucview for 90 min at 37 °C and fixed with 4% (w/v) formaldehyde with 4% (w/v) sucrose in PBS for 20 min. The samples were mounted in Prolong® Gold antifade reagent containing DAPI (Cat. #P36935, Life Technologies).

2.8. Cell proliferation

Alginate microcapsules were dissolved in chelating solution (10 mM HEPES pH 7.4 with 100 mM EDTA) and centrifuged either at 50 × *g* for 1 min to recover the tumour spheroids or at 400 × *g* for 5 min to recover all the cell components. Pellets were solubilized in water subjected to ultra-sounds to lyse cells. Cell proliferation was measured by the amount of DNA present in the samples using Quant-iT™ PicoGreen® dsDNA Assay Kit (Invitrogen). DNA quantification was used to quantify the number of cells throughout the culture and in drug studies.

Cell proliferation was also assessed by the incorporation of Click-iT® EdU (Life Technologies) during DNA replication, according

to manufacturer's instructions. Alginate microcapsules were incubated overnight with 10 μM of EdU and fixed with 4% (w/v) formaldehyde with 4% (w/v) sucrose in PBS for 20 min. The samples were mounted in Prolong® Gold antifade reagent containing DAPI (Life Technologies) and the fluorescence was analyzed in an Andor spinning disk microscope (Revolution XD, Andor).

2.9. Metabolic activity

The reduction capacity of the cultures was measured by PrestoBlue™ Viability Reagent reduction assay (Cat. #A13262, Life Technologies), according to the manufacturer's instruction. The samples were incubated with 1× Presto blue for 30 min at 37 °C and the fluorescence was read at 560 nm excitation and 590 nm emission in the micro plate reader Infinite®200 PRO (NanoQuant, Tecan Trading AG).

ATP levels were measured by CellTiter–Glo® 3D Cell Viability Assay (Promega) according to the manufacturer's instructions. Cell media was removed from each well and capsules were dissolved and centrifuged for 3 min at 500 × *g*. Subsequently, equal volumes of CellTiter-Glo® reagent and the correspondent media were added to the wells. Plates were incubated at room temperature for 120 min on a shaker and luminescence was measured in the micro plate reader Infinite®200 PRO (NanoQuant, Tecan Trading AG).

2.10. Immunofluorescence microscopy

Samples were collected and fixed in 4% (w/v) formaldehyde with 4% (w/v) sucrose in PBS for 20 min. Then, they were dehydrated in 30% (w/v) sucrose for approximately 5 h and embedded in Tissue-Tek® O·C.T. (Sakura) and frozen at −80C for cryosectioning. The frozen samples were sliced with a thickness of 10 μm in a cryostat (Cryostat CM 3050 S, Leica). The cryosections were permeabilized for 10 min with 0.1% (v/v) Triton X- 100 (Sigma-Aldrich), blocked with 0.2% (w/v) fish-skin gelatin (FSG; Sigma-Aldrich) in PBS for 30 min. Primary and secondary antibodies were prepared in 0.125% (w/v) of FSG in PBS and incubated for 2 or 1.5 h. The samples were mounted in Prolong® Gold antifade reagent containing DAPI (Life Technologies). The primary antibodies used were anti-collagen type I, IV, fibronectin, vimentin (all from Abcam), N-cadherin (R&D systems), E-cadherin (Santa Cruz Biotechnology) and phalloidin for detection of F-actin (Invitrogen). Samples were visualized using a fluorescence microscope (DMRB6000, Leica).

2.11. Light-sheet fluorescence microscopy

The custom-made light-sheet microscope used for these experiments is an evolution of the SPIM-Fluid system [40]. CW lasers with excitation wavelengths of 488 nm (Cobolt, MLD 50 mW), 515 nm (TOPTICA, iBeam Smart 515-S 100 mW) and 637 nm (Cobolt, MLD 150 mW) are used for excitation. The light sheet is created by a pair of galvanometric mirrors (Thorlabs, GVSM002), conjugated with the illumination objectives (Nikon, PlanFluor 4×, NA 0.13). We use a 50/50 beamsplitter cube (Thorlabs, CCM1-BS013) to create double side illumination, increasing the quality of the images. On each arm, laser beams are expanded using a telescope system, composed of two achromatic doublets (Thorlabs, AC254-050-A-ML (f = 50 mm) and AC254-200-A-ML (f = 200 mm)), creating a flat top Gaussian beam profile. A relay lens set, with two achromatic lenses (Thorlabs, AC254-075-A-ML (f = 75 mm)) is used in the right arm, so the planes are properly conjugated.

Detection is performed in an up-right configuration, using water dipping objectives (Nikon, PlanFluor 10×, NA 0.3). An achromatic doublet (AC254-200-A-ML) forms an image onto a Hamamatsu Orca Flash4.0 cMOS camera chip. Different emissions filters (Chroma and Semrock: 520/15 (GFP), 590/50 (dtTomato), 638LP (Cell tracker deep red)) are selected using a motorized filter wheel (Thorlabs, FW102C).

Samples were fixed as described above, and directly imaged without any further manipulation. In order to increase the throughput of the system, samples are loaded into FEP tubes (which refractive index is matched to water, 1.33) and transported towards the detection objective field of view using a syringe pump (Tecan, Cavro Centris). Scanning of the encapsulated aggregates is performed by vertical translation of the tubes, using a motorized stage (PI M-501.1DG), through a fixed horizontal light sheet plane. This allowed a straightforward the evaluation of hundreds of 3D-3-cultures with different co-culture combination and at different time points. All the components of the microscope are controlled using the custom-made software (LabView) and the image processing is carried on Fiji.

2.12. Immunohistochemistry

Samples were fixed as described above and embedded in 1% (w/v) high melting temperature agarose (Lonza), dehydrated in graded alcohols and then embedded in paraffin wax. Paraffin blocks were sectioned (3 mm) for Hematoxylin & Eosin and immunohistochemical staining. Immunohistochemistry was carried out in a BenchMark ULTRA Automated IHC/ISH slide staining system from Ventana Medical Systems, Inc. According to instrument specifications. Briefly, antigen retrieval was performed in the instruments using the standard antigen retrieval solutions. Staining was performed using as primary antibodies the following clones: Anti-CD45 (clone 2B11 + PD7/26 from Agilent/DAKO), CD68 PG-M1 clone PGM1 from Agilent/DAKO and CD163 (clone 10D6 from Leica Biosystems). OptiView DAB IHC Detection Kit from Ventana Medical Systems, Inc. was used as the visualization system for all. Sections of human tonsil were included in all slides as positive and negative controls. The resulting staining was evaluated by bright field microscopy. Quantification was performed using the image analysis software Image J, by applying the colour deconvolution plug-in and determining the DAB-positive and negative areas. The results are expressed as the percentage of positive staining within the alginate capsule.

2.13. Flow cytometry

Alginate microcapsules were dissolved with a chelating solution as indicated above and centrifuged at 600 × *g* for 5 min. To analyze the surface expression of immune cells, CD45 (Cat. #555483, BD Pharmingen™, San Diego, USA), CD163 (Cat. #FAB1607A, R&D Systems) and CD206 (Cat. #321114, Biolegend) were used. The cell suspensions were incubated with the primary antibodies conjugated with a fluorophore for 45 min in PBS. The samples were centrifuged, washed and analyzed in a CyFlow space (Partec).

2.14. Cytokine analysis

Supernatant media were collected at day 7 and day 21 and centrifuged at 1000 xg for 5 min. Samples were snap-frozen and stored at −80 °C until use. The Bio-Plex Pro™ Human Chemokine Panel, 40-Plex #171AK99MR2 was applied and samples were analyzed in a Bio-Plex® 200 System according to the manufacturer's protocol (http://www.bio-rad.com/webroot/web/pdf/lsr/literature/10031990.pdf).

2.15. Gene expression analysis

Alginate microcapsules were dissolved with a chelating solution as indicated above, centrifuged at 400 × *g* for 5 min. Pellets were snap-frozen and kept at −80 °C until RNA isolation. Total RNA was extracted from samples with the High Pure Isolation kit (Roche) and then converted to cDNA with Transcriptor High Fidelity cDNA synthesis kit (Roche), both according to the manufacturer's instructions. Real Time-PCR was performed using SYBR-Green (SYBR Green I Master Kit, Roche) in LightCycler 480 (Roche). Gene expression calculations were based in relative quantification using the comparative CT method ($2^{-\Delta\Delta CT}$) and RPL22 and HPRT1 endogenous expression were used as controls. The sequences of the primers used are listed in supplementary Table 1.

3. Results

3.1. Advanced stage NSCLC spheroids maintain mesenchymal phenotype in 3D-3-culture

With the goal of establishing *in vitro* tumour models of NSCLC that incorporate the myeloid compartment found at the tumour site, 3D-3-cultures were established. Our strategy employed alginate microencapsulation and stirred culture described previously by our group [25,28], and summarized in Fig. 1 A. The 3D-3-cultures were set up within alginate microcapsules of an average diameter of 652 ± 26 μm, with three cellular compartments – NSCLC (NCI-H157) tumour spheroids, CAF and a monocytic cell line (THP-1) (Fig. 1 B). Microencapsulated cells were maintained in stirred suspension culture for up to three weeks and presented high viability throughout culture time (Fig. 1C). Cell proliferation was homogeneous within the tumour spheroids and also in the remaining cellular compartments, as evidenced by Edu staining (Fig. 2 A). Cell proliferation resulted in a 10-fold increase in tumour cell concentration by week 3 (Fig. 2 B), which was comparable to tumour cell growth in monocultures and in double co-culture controls. Even though no statistical differences in the average spheroid diameter were observed between the 1st and 3rd weeks of culture, the number of spheroids per capsule increased over time and a high dispersion in the average diameter of spheroids was observed in the 3rd week of culture (supplementary Fig. 1), which is in line with the increase in cell concentration. These results suggest that the presence of stromal and monocytic cell types had no major effect on tumour proliferation and that there were no nutrient or spatial restrictions within the microcapsules.

Along the culture period, multiple spheroids and clusters of cells were found spread within the microcapsules in 3D-3-cultures, constituted by tumour, CAF and THP-1 cells (Fig. 1 B; 2 A and supplementary video). In contrast, 1–3 large spheroids were found in the microcapsules of tumour monocultures (Fig. 2 A). Tumour spheroids within 3D-3-cultures were composed of cells positive for N-cadherin and vimentin, with low E-cadherin expression (data not shown) and presented loose cell architecture, as evidenced by F-actin staining (Fig. 2C), showing that NCI-H157 cells maintain

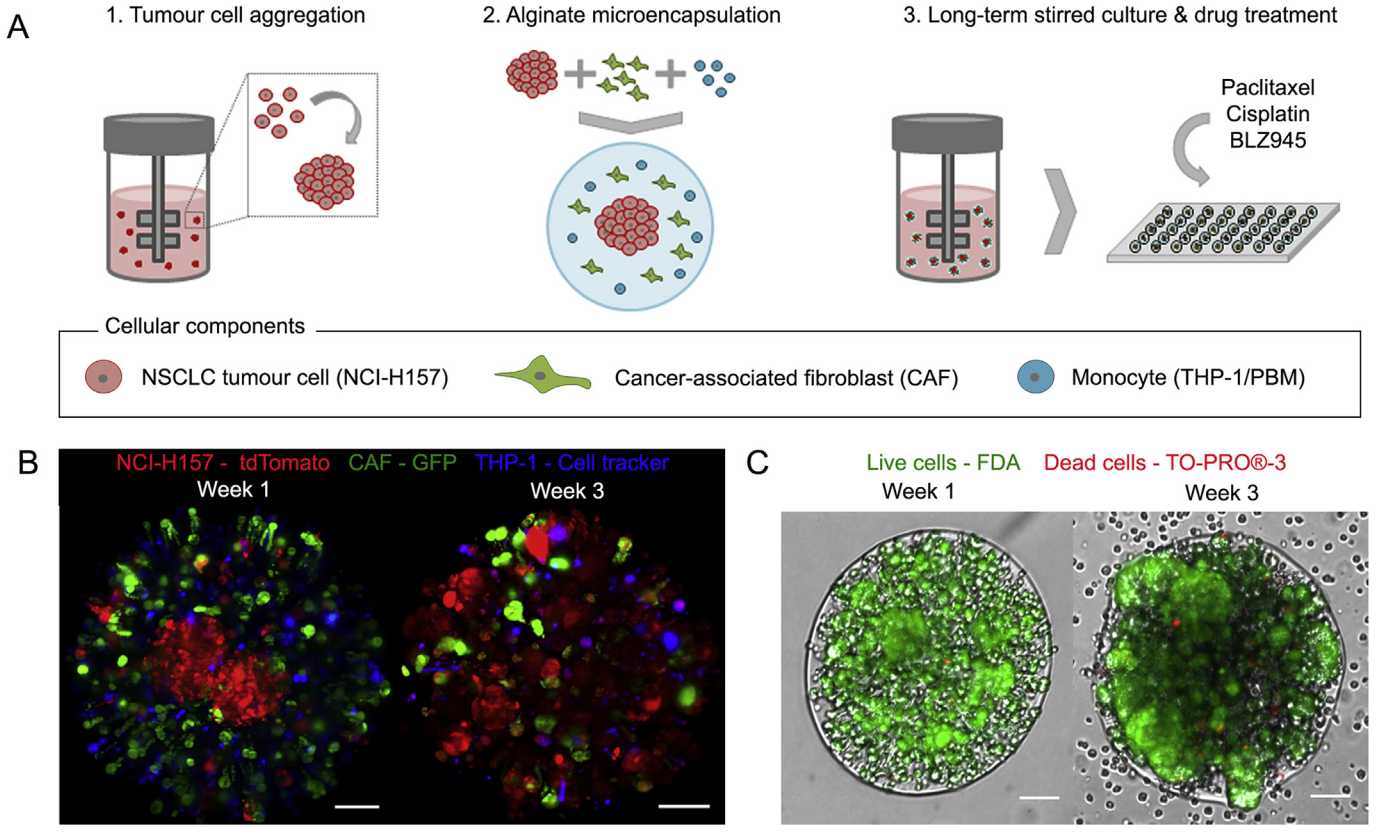

Fig. 1. - Experimental approach and culture monitoring over time. (A) Schematic representation of the experimental approach: 1 - Tumour cells were inoculated as single cells in stirred-tank vessels to promote cell aggregation. 2 - After 3 days, tumour spheroids and single cells of CAF and THP-1 or PBM were mixed and encapsulated in alginate, resulting in microcapsules enclosing the three cellular components. 3 - The alginate microcapsules were maintained in long-term culture while culture characterization and drug treatments were performed. The representation is not to scale. (B) Alginate microcapsules of the 3D-3-cultures in the 1st and 3rd week of culture visualized by light-sheet fluorescence microscopy. The cellular types are labelled by tdTomato (red) – NSCLC spheroids; GFP (green) – CAF; Cell tracker™ (blue) – THP-1. (C) Live/dead assay of 3D-3-cultures in the 1st and 3rd week of culture: FDA (green) – live cells; TO-PRO-3 (red) – dead cells. Scale bars represent 100 μm.

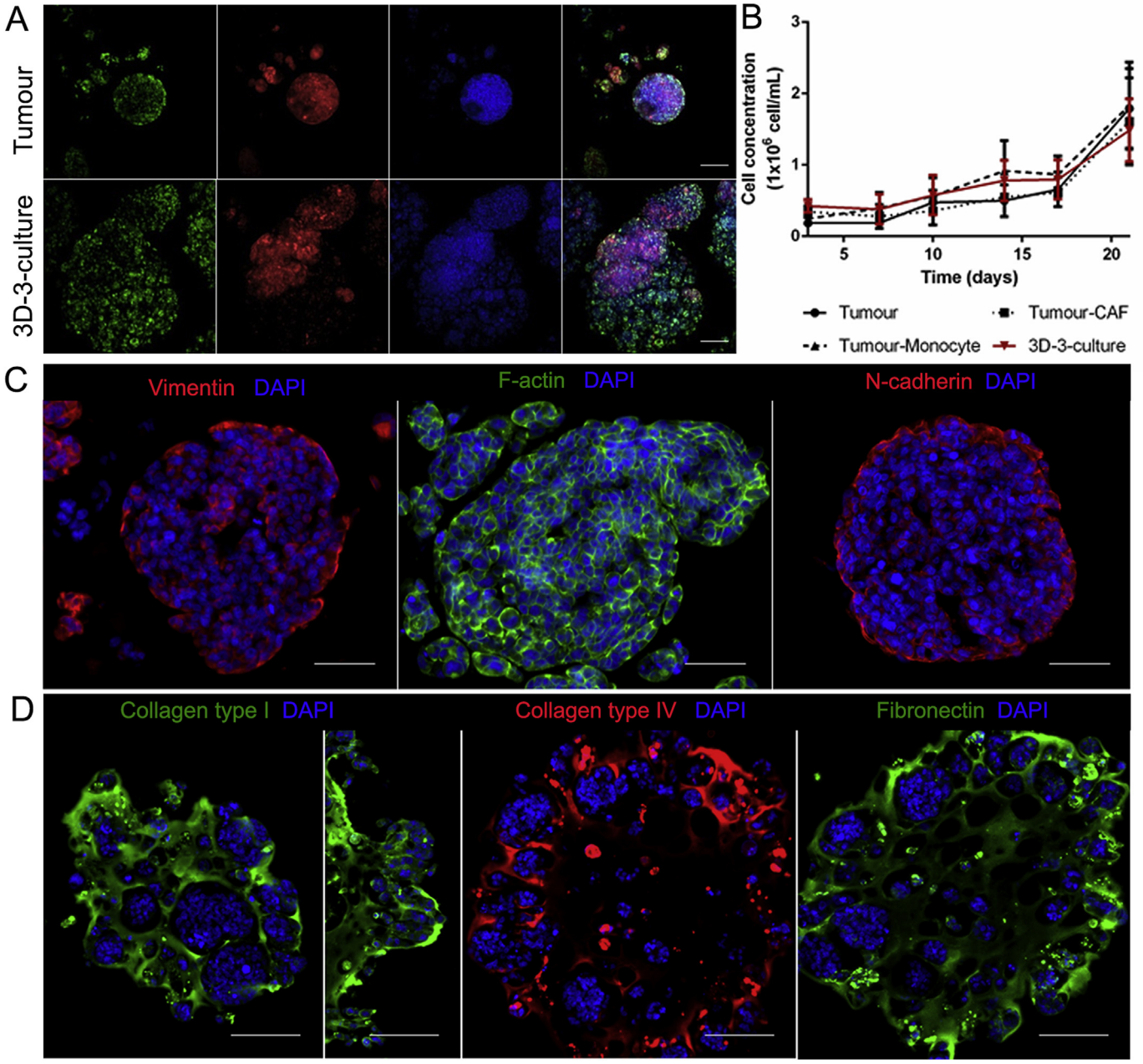

Fig. 2. - Phenotypic characterization of tumour spheroids and ECM accumulation in alginate microcapsules. (A) Cell proliferation and morphology of tumour spheroids in mono- (upper panel) and 3D-3-cultures (lower panel) at day 14 of culture. From the left: Edu (green) – proliferative cells; tdTomato (red) - NCI-H157; DAPI (blue) – Nuclei and merge of all channels. (B) Tumour cell concentration profile of mono-, double co-cultures and 3D-3-culture along 3 weeks of culture; data are mean ± SEM from three independent experiments. (C–D) Immunofluorescence microscopy of 3D-3-culture alginate microcapsules in 10 μm thick cryosections, at day 21, of (C) Tumour cells: Vimentin (red), F-actin (Phalloidin; green); N-cadherin (red) and Nuclei (DAPI; blue). Scale bars represent 50 μm and (D) ECM: Collagen type I (green), Collagen type IV (red), Fibronectin (green) and Nuclei (DAPI; blue). Scale bars represent 100 μm.

their typical mesenchymal phenotype upon microencapsulated spheroid culture. Moreover, collagen type I (Col I), collagen type IV (Col IV) and Fibronectin (FN) accumulated in the alginate microcapsules intercalated with cell spheroids, clusters and single cells, in a tissue-like phenotype (Fig. 2 D). The accumulation of ECM (*e.g.* Col I) was marked in the edges of the alginate microcapsules, in which the cells aligned in between the collagen fibres, displaying a migratory phenotype. These results suggest that the model set up was permissive to cell movement within the microcapsules, accommodating cell-cell interactions occurring between the different cell compartments, which may be promoted by the ECM accumulation [41,42].

Supplementary video related to this article can be found at https://doi.org/10.1016/j.biomaterials.2018.02.030.

3.2. Myeloid cells infiltrate into the tumour spheroids and display a TAM-like phenotype

To fully assess the model's capability of recapitulating the immune contexture, namely the trans-polarization of monocytic THP-1 cells into myeloid M2-like macrophages and their infiltration into human NSCLC tumours, the M2-like macrophage population was characterized in detail.

$CD45^+$ (protein tyrosine phosphatase, receptor type, C/PTPRC;

pan leukocyte marker) cells were detected in small clusters around larger tumour spheroids and as single cells dispersed in between the latter, both in 3D-3-cultures and in tumour-immune co-culture controls (Fig. 3 A). Furthermore, the presence of $CD45^+$ cells distributed within tumour spheroids suggests that alginate microcapsules allow cell migration and that the generated TME within the microcapsules drives the infiltration of myeloid cells into the tumour spheroids. The immunohistological staining of CD68 (Cluster of Differentiation 68) (Fig. 3 A), which is highly expressed in tissue macrophages, was similar to CD45. CD68 expression together with cell morphology supports differentiation of most monocytes into macrophages.

Cells positive for CD163 (scavenger receptor for the haemoglobin-haptoglobin complex), an M2-like macrophage marker, were detected in 3D-3-cultures (Fig. 3 A). $CD163^+$ cells could also be detected in tumour-immune and in CAF-immune co-cultures but in THP-1 monocultures only residual levels were detected (Fig. 3 A and supplementary Table 2). This data suggests that the presence of both NCI-H157 spheroids and CAF are required to promote the differentiation of monocytic cells towards M2-like macrophages and that polarization of THP-1 cells depends on the interaction with other cell types. The proportion of M2 differentiation (ratio $CD163^+/CD68^+$ cells) is approximately 15–20% in 3D-3-cultures and tumour-monocyte and only 2% in CAF-monocyte cultures. While most of the $CD45^+$ cells were detected in clusters, on the edges and inside the spheroids, $CD163^+$ cells were mostly infiltrated in tumour spheroids (Fig. 3 A).

We also analyzed the secretory profile of the cultures, screening for the presence of cytokines and chemokines associated with immunosuppressive environment and invasive phenotype (Fig. 3 B). Tumour cells in monoculture secreted IL4, IL13, IL10 and CXCL1 cytokines, previously described as associated with macrophage recruitment and induction of an M2-like activation state [43–47]. Moreover, in 3D-3-cultures, there was an increased secretion of metalloproteinase-9 (MMP9) and of cytokines typically expressed by M2-like macrophages, namely CCL22 and CCL24 [48–50]. The secretion profile and immunodetection show that M2-like macrophages are present in 3D-3-cultures.

We also established 3D-3-culture models with donor-derived peripheral blood monocytes (PBM), isolated from peripheral blood mononuclear cells (PBMC). PBM maintained high cell viability over 7 days when cultured as 3D-3-cultures. After 4 days, approximately 70–80% of $CD45^+$ cells expressed the M2-like markers CD206 and CD163 while in microencapsulated monocultures (Microencapsulated PBM) this percentage was significantly lower, around 2–6% (Fig. 3C). In comparison with the 2D cultures (2D PBM), the differences in percentage of differentiated cells were less evident, although median fluorescence intensity of each marker was higher in 3D-3-culture (Sup. Fig. 2). This suggests that the phenotype of the macrophages expressing M2-like markers was different, pointing to a higher maturation in the 3D-3-culture. Altogether, these observations indicate that not only an immortalized monocytic cell line but also primary monocytes polarize into M2-like macrophages in the 3D-3-culture setup.

3.3. Effects of chemo- and immunotherapies can be assessed in 3D-3-culture

As proof-of-concept that the 3D-3-culture setup allows the study of the effect of drugs in an immunity relevant context, we challenged it with Cisplatin and Paclitaxel, two chemotherapeutic drugs routinely used in the treatment of NSCLC [51,52], as well as BLZ945, an immunomodulatory drug targeting CSF1R (Colony Stimulating Factor 1 Receptor) [16,17,53,54]. This receptor was upregulated over time in 3D-3-culture (data not shown) and previous reports showed that its inhibition leads to decreased proliferation of BM-derived monocytes and promotes repolarization of M2-like macrophages into an M1-like phenotype [15,16].

Dose-response curves for Cisplatin and Paclitaxel were established for tumour monocultures and the IC_{50} value was determined by measuring ATP levels and confirmed through additional readouts (resazurin reduction and DNA quantification) (Sup. Fig. 3).

Treatment with Paclitaxel led to a reduction of the ATP levels of tumour, CAF and monocyte monocultures, which ranged from 58 to 37% of the control (Fig. 4 A). The 3D-3-culture and CAF-monocyte co-culture presented a metabolic activity of approximately 80% upon treatment, showing less sensitivity to the drug comparing with the mono-culture (Fig. 4 A and sup. Fig. 4 A). The lower drug response in 3D-3-cultures reflects the lower induction of apoptosis throughout the cultures, as observed by Nucview™ fluorescence staining (Fig. 4C and sup. Fig. 4 A, C). Nevertheless, proliferating cells could still be detected in 3D-3-cultures, as well as in co-culture controls, in tumour spheroids and in the stromal and immune compartments. These data suggest that there is a subset of tumour and immune cells not affected by the drug (Fig. 4 D).

In contrast to what was observed for Paclitaxel, no significant differences were observed between the metabolic activity of tumour monoculture and the 3D-3-culture upon treatment with Cisplatin (Fig. 4 B). The ATP levels of monocyte and CAF monocultures, as well as monocyte-CAF co-cultures ranged from 7 to 23% of the control, showing that all cell compartments were affected by the treatment (Fig. 4 B). The generalized effect of cisplatin was also evident in the apoptosis fluorescence staining, in which apoptotic cells can be observed throughout the tumour, stromal and immune compartments (Fig. 4C and sup. Fig. 5C). Concomitantly, hardly any proliferative cells were detected after treatment in the 3D-3-culture (Fig. 4 D).

Concerning BLZ945 treatment, there were no significant alterations in ATP levels in THP-1 and tumour monocultures relative to the non-treated controls (Fig. 5 A), suggesting that the concentrations employed were not acting through generalized toxicity mechanisms. BLZ945 induced a decrease in CD163 gene expression in 3D-3-cultures after drug treatment and an increase in the expression of the M1-associated gene CCR7 (C-C chemokine receptor type 7; Fig. 5 B). The expression of PTPRC (CD45) also increased up to 2-fold, although there was no evidence of alteration of the numbers of immune cells either due to apoptosis or proliferation (Fig. 5 B). Gene expression of CSF1R increased up to 1.8-fold (Fig. 5 B), in accordance to what has been previously reported in cultured primary monocytes [15].

CCR7 gene expression also increased after cisplatin treatment, while expression of CD68 and CD163 remains unchanged (Fig. 5 B). This may suggest that, in addition to the depletion of immune cells, the phenotype of the surviving macrophage population is also modulated in cisplatin-treated cultures. In fact, several reports have indicated that cisplatin plays a role in immunomodulation, specifically by altering the ratio of M2/M1-like macrophages [55,56].

In PBM-3D-3-cultures treated with 1×10^{-6} M of BLZ945, there was a reduction of up to 39% of $CD206^+$ cells and up to 45% reduction in $CD163^+$ cells (Fig. 5C). These results suggest that the treatment with BLZ945 leads to a decrease in the M2-like macrophage population in 3D-3-cultures both with the THP-1 cell line and with PBM, which may be attributed to a repolarization from M2-to the M1-like macrophage phenotype, as previously reported [15,16]. This repolarization of the macrophage compartment did not have a significant impact on the viability of tumour cells in 3D-3-culture (Fig. 5 A, D). Nevertheless, the results demonstrate that our model is suitable to perform immunomodulation studies *in vitro*, allowing the depiction of specific effects on each cellular component.

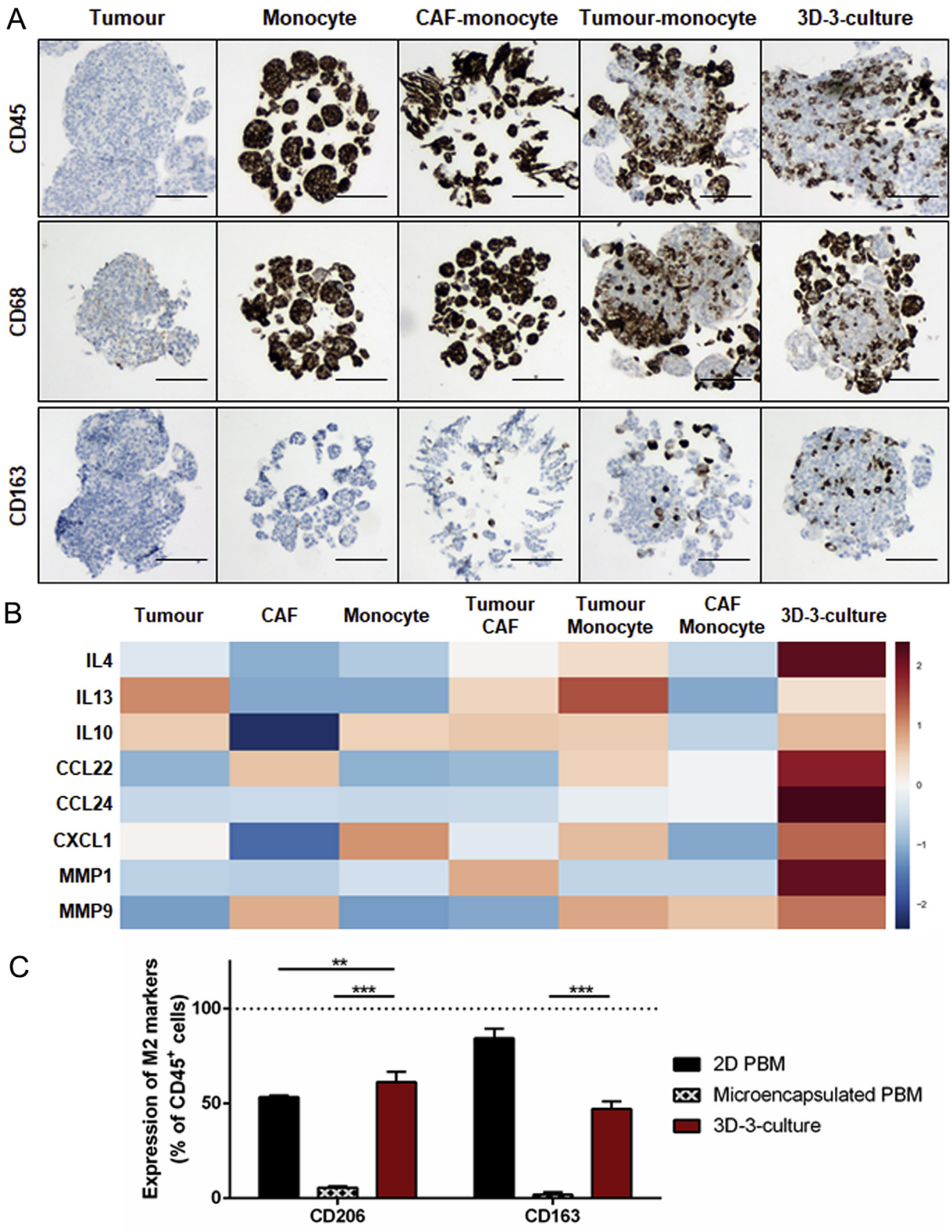

Fig. 3. - Characterization of the immunosuppressive TME in 3D-3-cultures. (A) Immunohistochemistry staining of alginate microcapsules in 3 μm thick paraffin sections after 3 weeks of culture with the immune markers CD45, CD68 PG-M1 and CD163. From the left: Tumour and monocyte mono-cultures, CAF-monocyte and tumour-monocyte double co-cultures and 3D-3-culture. Scale bars represent 100 μm. (B) Heatmap of the cytokine profile of IL4, IL13, IL10, CCL22, CCL24, CXCL1, MMP1 and MMP9, represented in z-score. From left: Mono-cultures of tumour, CAF and monocytes, double co-cultures of tumour-CAF, tumour-monocyte, CAF-monocyte and 3D-3-culture. All the proteins presented had a significant differential expression ($p \leq 0.05$) by ANOVA analysis. (C) Immunodetection of cells double positive for the leucocyte marker CD45 and M2-associated markers CD163 and CD206 of peripheral blood derived macrophages 4 days after isolation in monolayer mono-culture (2D PBM) and microencapsulated mono-culture (Microencapsulated PBM) and in 3D-3-cultures (with tumour cells and CAF). Data are mean ± SEM from up to six independent experiments. * indicate significant differences between different cultures; (***$p < 0.001$; **$p < 0.01$) by an unpaired t-student test.

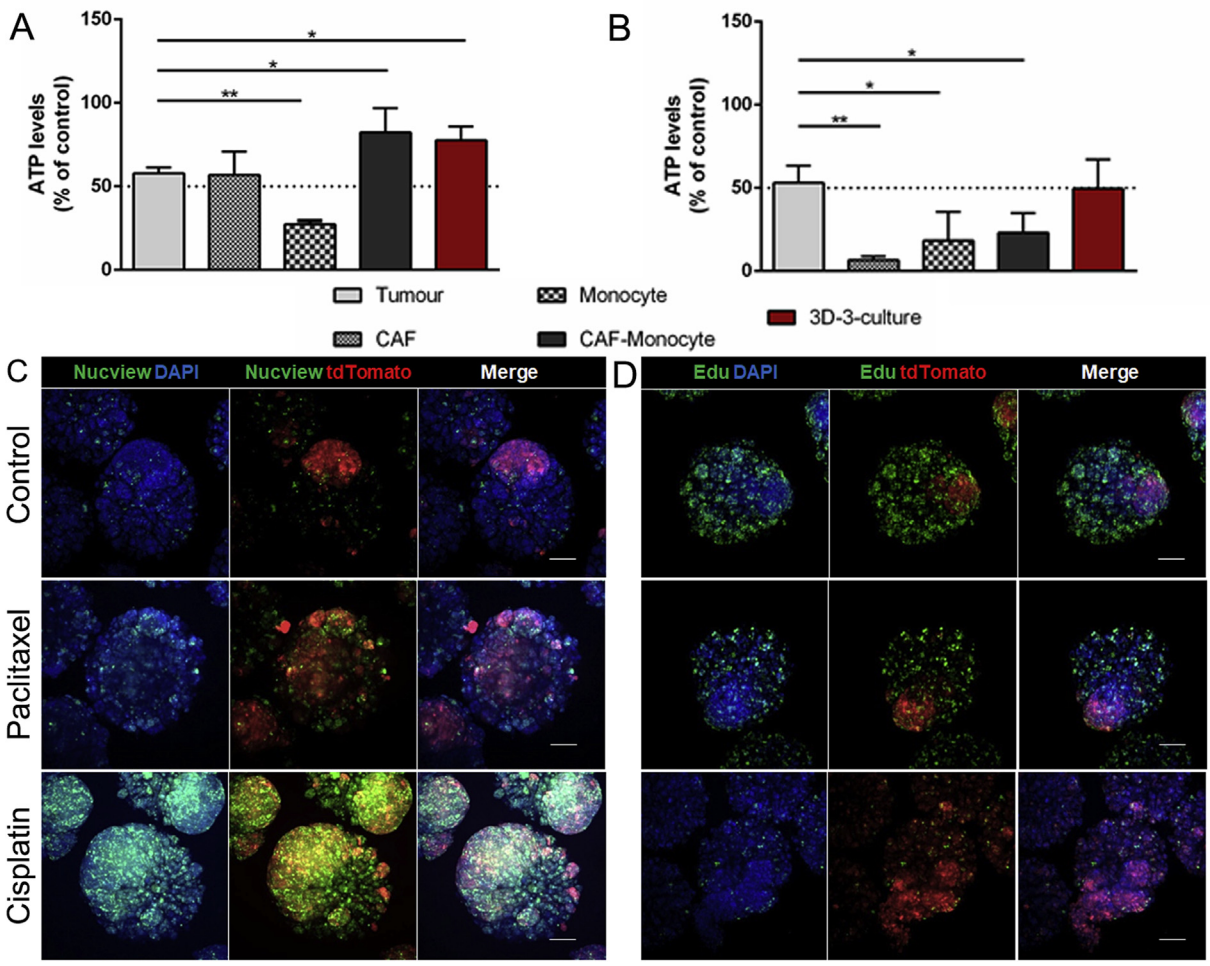

Fig. 4. - Chemotherapeutic treatment in 3D-3-culture. Metabolic activity (ATP levels) of (A) Paclitaxel (10^{-8} M) and (B) Cisplatin (10^{-5} M) treated mono-cultures of tumour, monocyte and CAF, double co-culture of CAF-monocyte and 3D-3-culture. Data are mean ± SEM from three independent experiments. * indicate significant differences between tumour and other cultures by an unpaired t-student test (**$p < 0.01$, *$p < 0.05$). Immunofluorescence images of 3D-3-culture after treatment and respective controls for analysis of (C) apoptosis: Nucview (green) - apoptotic cells; tdTomato (red) – NCI-H157; DAPI (blue) - nuclei; and (D) proliferation: Edu (green) - proliferative cells; tdTomato (red) – NCI-H157; DAPI (blue) – nuclei. Scale bars represent 100 μm.

4. Discussion

Extensive studies have shown that the tumour microenvironment (TME) is important for disease progression and drug response, however, its integration into drug screening platforms has been difficult due to the lack of cellular models amenable for throughput screening. In this work, we describe the development of a 3D-3-culture system, combining alginate microencapsulation and stirred culture, which incorporates tumour spheroids, cancer-associated fibroblasts and trans-polarized macrophages in an environment where the dynamic interaction between each compartment is recapitulated. Our results demonstrate that the 3D-3-culture allows polarization of a monocytic cell line (THP-1) and peripheral blood-derived monocytes (PBM) into tumour-associated macrophages (TAM) and infiltration in the tumour tissue, which can be modulated upon exposure to chemotherapeutic and immunomodulatory drugs. This system allows the study of monocyte recruitment, as well as, phenotype induction in a robust system, with continuous monitoring and compatible with drug screening platforms.

In the 3D-3-culture, NCI-H157 tumour cells maintained their proliferative state and displayed phenotypic markers typical of aggressive stages of NSCLC, such as expression of N-cadherin and vimentin, coupled with low expression of E-cadherin. This pattern, typical of late-stage epithelial-to-mesenchymal transition, was also described for immunohistochemical analysis of human tissue samples from primary tumours of lung squamous cell carcinoma and correlates with advanced stage tumours [57]. Although no major differences in the proliferation and histological markers of tumour cells were observed upon co-cultivation with CAF and myeloid cells, there was an evident spatial remodelling of the different cell compartments within the alginate microcapsules over the course of the culture. This can be attributed to the ECM accumulation observed within the microcapsules (Col I, IV and FN) and the secretion of metalloproteinases (MMP1 and MMP9) and suggests an increased invasive phenotype in the 3D-3-culture. This secretory profile was previously described for co-cultures of tumour cells, fibroblasts and macrophages, and is associated with the acquisition of higher metastatic potential [33,58].

The 3D-3-culture model allowed for the recapitulation of key hallmarks of lung cancer immune microenvironment. Early reports indicate that spheroids are suitable for tumour-immune interaction studies [59,60], as tumour architecture is important in establishing the immunosuppressive TME found in human tumours [61–64]. In the 3D-3-culture, CD68 and $CD163^{+}$ cells were detected, pointing to macrophage polarization into an M2-like phenotype, as

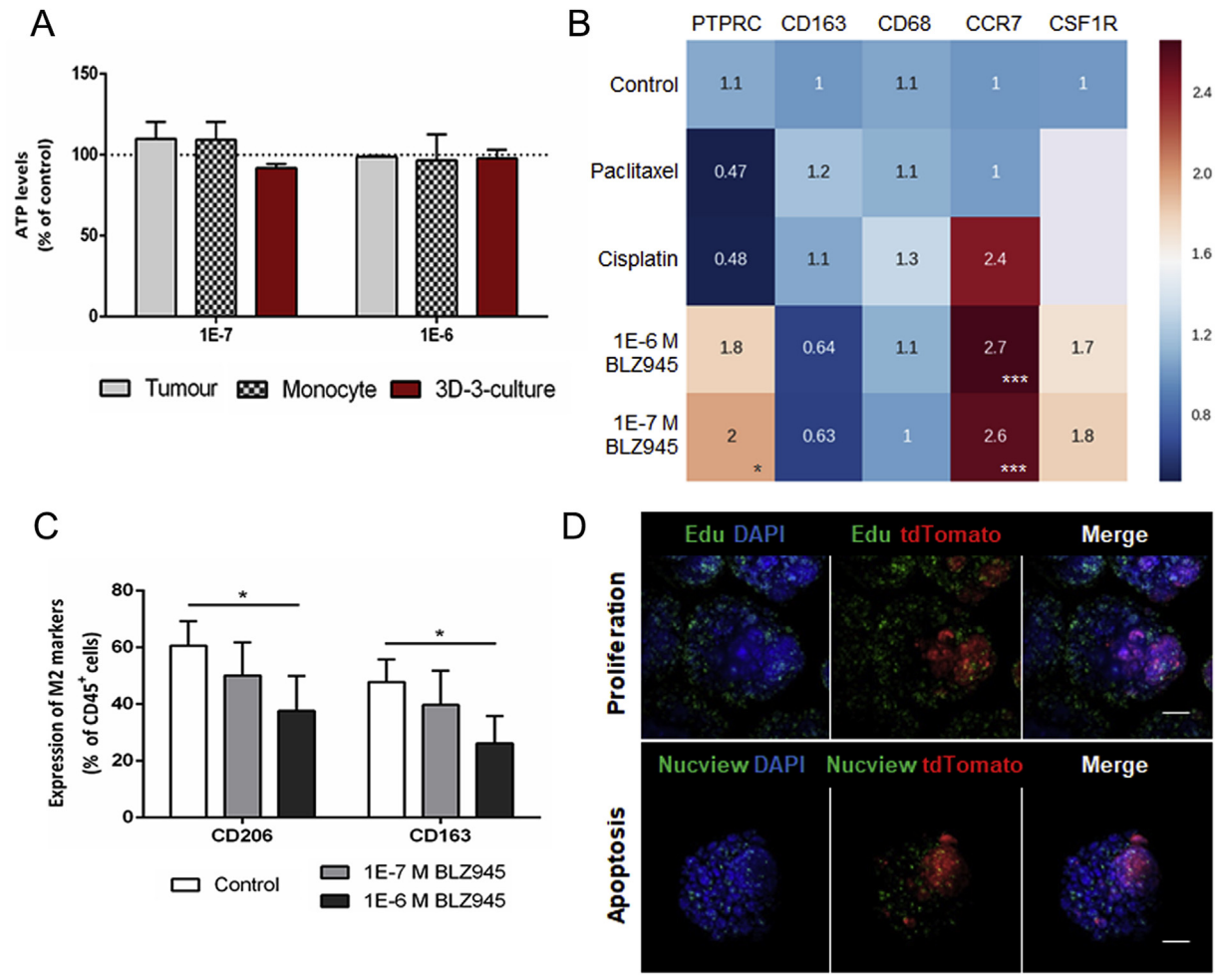

Fig. 5. - Immunotherapeutic treatment in 3D-3-culture. (A) Metabolic activity (ATP levels) of cultures after treatment with 10^{-7} and 10^{-6} M of BLZ945 in tumour and monocyte mono-cultures and 3D-3-culture. Data are mean ± SEM for three independent experiments. (B) Heatmap with fold increase in gene expression of macrophage markers after treatment with chemotherapeutic and immunotherapeutic drugs in 3D-3-culture, relatively to the non-treated controls. Data are mean from three independent experiments. * indicate significant differences of treated conditions to control by a two-way ANOVA and a Sidak's multiple comparison test (***$p < 0.001$, *$p < 0.05$). (C) Immunodetection of cells double positive for the leucocyte marker CD45 and M2-associated markers CD163 and CD206 of 3D-3-cultures with donor-derived monocytes with and without treatment with BLZ945 (10^{-7} and 10^{-6} M). Data are mean ± SEM from three independent experiments. * indicate significant differences between treated conditions and control by a paired t-student test (*$p < 0.05$). (D) Immunofluorescence images of (10^{-6} M) BLZ945 treated 3D-3-cultures, showing apoptosis in the upper panel: Nucview (green) - apoptotic cells; tdTomato (red) – NCI-H157; DAPI (blue) - nuclei; and proliferation in the lower panel: Edu (green) - proliferative cells; tdTomato (red) – NCI-H157; DAPI (blue) – nuclei. Scale bars represent 100 μm.

described for primary tumours of NSCLC [65,66]. Moreover, a high proportion of $CD163^+$ cells was detected within tumour spheroids, demonstrating that the developed model was conducive to cell migration, as occurs with the myeloid infiltrate in human lung cancers. The detection of $CD163^+$ cells was also observed in tumour-immune and CAF-immune co-culture controls, however, at lower level. This is in line with previous reports suggesting that the stromal compartment is also primarily involved in the recruitment and activation of monocytes in the TME [67], as CAF exhibit an activated fibroblast phenotype, with altered secretory profile and ECM production [23,68]. In fact, in co-culture models of blood monocytes with breast cancer or CAF spheroids, monocyte migration was higher towards CAF spheroids, a phenotype linked to overexpression of CCL2 [69].

A significant feature of the developed 3D-3-culture model for tumour modelling is the use of an inert scaffold, as the introduction of physiologically relevant ECM remains a fundamental challenge for tumour modelling in current *in vitro* settings [20]. Routinely used Matrigel or collagen-based artificial ECM substrates do not represent the predominant ECM proteins found in the target tissue [20]. We demonstrate that the alginate microcapsules allow the accumulation of collagen type I and IV, forming collagen fibres that intercalate cells, and fibronectin, resembling the tissue architecture and contributing to the migration and tissue remodelling within the microcapsules. This cell remodelling allows cell interactions to occur naturally, resulting in a cell distribution within the alginate microcapsules that presents features existent in the human tissue of NSCLC patients, such as macrophage infiltration and extravasation of tumour cells to the surrounding stroma [70].

The accumulation of a cocktail of soluble factors plus the cell-cell interactions observed have a key role in modulating the phenotype of macrophages in the 3D-3-culture model, since the polarization of macrophages was not promoted by the supplementation with cytokines. In a previous work, we have also shown that alginate capsules can accumulate soluble factors such as IL6, IL8, CXCL1, Serpin [28]. Here, analysis of the secretory profile in the 3D-3-culture model evidenced the formation of an immunosuppressive environment. Therefore, the induction of an M2-like phenotype observed may be explained by the accumulation of IL4, IL13, IL10 and CXCL1, cytokines previously described to

contribute to the referred phenotype [45–47]. Furthermore, a specific accumulation of CCL22 and CCL24 in week three of the 3D-3-cultures was observed. Both cytokines were previously reported to be produced by TAM and are involved in the recruitment and differentiation of regulatory T cells to the TME, which correlate with poor prognosis and suppress antitumour-specific immune responses [14,50,71]. MMP9 was also upregulated primarily in 3D-3-cultures. This metalloprotease was reported to be expressed by TAM from primary lung cancer tissue and its expression is correlated with disease progression in NSCLC patients [72]. Recent reports also highlight the important role of cell-cell interactions. Specifically, binding of tumour-associated mucin O-glycans to lectin receptors on immune cells may promote immune-tolerance and emergence of immune-resistant cancer cell variants [73,74] [75,76]. These studies were important to help dissect the TAM inducing stimuli, however, these were mainly conducted in models where the TME complexity is not represented (tumour cell monocultures), in a non-human setting (GEMM models) or using targeted approaches towards identifying the partners of previously described tumoral glycoconjugates or lectins. The developed 3D-3 model allows for cell-cell interaction between the different cell compartments. Therefore, it could be used to surpass some of the drawbacks of the above described models, and allow the dissection of the concerted action of both soluble factors and cell-cell interactions in response to a given stimuli, namely anticancer therapy.

The development of novel and improved therapeutics is an area of intense study in cancer research but still presents huge attrition rates. One of the limitations of current pre-clinical platforms is the lack of integration of multiple TME compartments. The use of platinum-based compounds, such as cisplatin, for chemotherapy has shown clinical efficacy against several solid tumours, including NSCLC [77]. Paclitaxel, a microtubule-stabilising agent, is another standard-of-care drug that induces cell death through interruption of mitosis [78]. Here we show that challenging our model with each compound led to different results. Although both drugs ultimately lead to cancer cell apoptosis, they present different mechanisms of action that might explain the different results obtained: paclitaxel is a microtubule stabilizer, whereas cisplatin crosslinks DNA [52,78]. Treatment with cisplatin led to a generalized tumour cell apoptosis, which was not affected by the presence of other cells in the TME. Paclitaxel, on the other hand, leads to a less extensive apoptosis induction in the 3D-3-culture than in mono-cultures, suggesting that the reciprocal interactions occurring between the stromal and immune compartment may alter cell's sensitivity to the drug. Such discrepancies are often observed when comparing response of *in vitro* drug screening platforms, devoid of TME, and *in vivo* drug sensitivity, highlighting the importance of incorporating the TME components when addressing drug response [79]. This shows that the developed model can aid in deciphering the microenvironmental regulation of therapeutic response. Moreover, the immunomodulatory effects of each chemotherapeutic agent could also be depicted. Cisplatin treatment led to a significant increase in CCR7 expression in the surviving macrophage population, which was not evident for paclitaxel treatment. In fact, increasing preclinical and clinical evidence has shown that cisplatin can modulate the immune system alone or in combination with immunotherapies [56]. Early studies had already linked cisplatin action to the activation of macrophages into an antitumoural state [80,81]. These findings demonstrated that cisplatin significantly increases antigen-presenting ability of murine macrophages. It also alters the macrophages' secretory profile. Costimulatory factors such as IL1, IL6, TNFα and NO, enhance autocrinally the antigen presenting and antitumour ability of other immune cells present in the TME [80,81]. More recently, adjuvant cisplatin chemotherapy increased antitumour efficacy through an increase of antigen specific $CD8^+$ cells systemically and intratumourally and by shifting the M1-/M2-like phenotype ratio in mice [82]. On the other hand, paclitaxel tumour reducing effects seem to also involve a direct stimulation of TAM's cytotoxicity [83,84] and cytokine release, namely IL-12, TNFα and iNOS by TAM [83,85]. However, its potential for inducing immunogenic cell death (ICD) by mitosis catastrophe-mediated tumour cell death is not fully understood [83].

Upon challenging the 3D-3-culture with the CSF1R inhibitor BLZ954, a significant decrease in the expression of CD206 and CD163 in the macrophage population was observed. CSF1R activation has been linked with proliferation and survival of macrophages, but also with the expression of M2-like genes [86]. Its inhibition is a promising anticancer strategy showing reduced tumour size and improved survival in a mouse breast tumour model [87] and leading to a significant clinical activity in patients [17]. Several reports have also shown that the effect of CSF1R inhibition in TAM could not only be dependent on macrophage depletion, but rather a repolarization into a more M1-like antitumour macrophage phenotype [16,54]. These effects could be recapitulated in our model which indicates that it is able to depict the immunomodulatory effects previously observed for mouse models in a human relevant TME context [16,54].

5. Conclusions

In conclusion, we have developed a 3D-3-culture model that mimics the dynamic interaction between tumour, stromal and immune compartments, alongside accumulation of ECM and secreted factors. This contributed to the maintenance of key features of advanced stage lung carcinoma, including the immunosuppressive environment. This model allowed the activation of monocytes into a TAM-associated phenotype without addition of external factors and the macrophage phenotype could be modulated upon treatment with immune-targeting and chemotherapeutic drugs. One of the main features of the 3D-3-culture system is that it is scalable, compatible with drug screening platforms and flexible, combining the use of cell lines with primary immune cells (PBM); this system is also transferable to other pathologies. Establishing *in vitro* models using cell lines enables the labelling of individual cell types. These models can be complemented with single cell imaging for tracking the response of specific cell compartments to a given stimuli, or with gene editing tools, such as CRISPR–Cas9 system, for the development of more translatable *in vitro* models of disease [20]. Nevertheless, this culture system may also be adapted to incorporate patient-derived tumour samples for *ex vivo* assessment of therapeutic efficacy using precision medicine approaches for translational research.

Data availability statement

The raw/processed data required to reproduce these findings cannot be shared at this time as the data also forms part of an ongoing study.

Acknowledgments

We gratefully acknowledge Vítor E. Santo for the discussions in the initial phase of the work. We acknowledge support from the Innovative Medicines Initiative (IMI) Joint Undertaking (grant agreement no. 115188), MINECO/FEDER, Spain (Severo Ochoa SEV-2015-0522, BIO2014-59614-JIN, RYC-2015-17935), Fundació Privada Cellex, Fundación Mig-Puig and CERCA program, Spain;

iNOVA4Health Research Unit (LISBOA-01-0145-FEDER-007344), which is cofunded by Fundação para a Ciência e Tecnologia (FCT)/ Ministério da Ciência e do Ensino Superior, through national funds, and by FEDER under the PT2020 Partnership Agreement, is also acknowledged. CP and MFE are recipients of PhDs fellowships SFRH/BD/52202/2013 and SFRH/BD/52208/2013, respectively, funded by FCT, Portugal.

Appendix A. Supplementary data

Supplementary data related to this article can be found at https://doi.org/10.1016/j.biomaterials.2018.02.030.

References

[1] A. Nyga, J. Neves, K. Stamati, et al., The next level of 3D tumour models: immunocompetence, Drug Discov. Today (2016), https://doi.org/10.1016/j.drudis.2016.04.010.
[2] D.F. Quail, J.A. Joyce, Microenvironmental regulation of tumor progression and metastasis, Nat. Med. 19 (2013) 1423–1437, https://doi.org/10.1038/nm.3394.
[3] V. Sathyanarayanan, S.S. Neelapu, Cancer immunotherapy: strategies for personalization and combinatorial approaches, Mol Oncol. 9 (2015) 2043–2053, https://doi.org/10.1016/j.molonc.2015.10.009.
[4] C. Feder-Mengus, S. Ghosh, A. Reschner, et al., New dimensions in tumor immunology: what does 3D culture reveal? Trends Mol. Med. 14 (2008) 333–340, https://doi.org/10.1016/j.molmed.2008.06.001.
[5] L. Jeanbart, M.A. Swartz, Engineering opportunities in cancer immunotherapy, Proc Natl Acad Sci. 112 (2015) 14467–14472, https://doi.org/10.1073/pnas.1508516112.
[6] M. Reck, D. Rodríguez-Abreu, A.G. Robinson, et al., Pembrolizumab versus chemotherapy for PD-L1–positive non–small-cell lung cancer, N. Engl. J. Med. 375 (2016) 1823–1833, https://doi.org/10.1056/NEJMoa1606774.
[7] H. Tang, J. Qiao, Y.-X. Fu, Immunotherapy and tumor microenvironment, Canc. Lett. 370 (2016) 85–90, https://doi.org/10.1016/j.canlet.2015.10.009.
[8] R.M. Bremnes, T. Dønnem, S. Al-Saad, et al., The role of tumor stroma in cancer progression and prognosis: emphasis on carcinoma-associated fibroblasts and non-small cell lung cancer, J. Thorac. Oncol. 6 (2011) 209–217, https://doi.org/10.1097/JTO.0b013e3181f8a1bd.
[9] J. Domagala-Kulawik, The role of the immune system in non-small cell lung carcinoma and potential for therapeutic intervention, Transl. Lung Cancer Res. 4 (2015) 177–190, https://doi.org/10.3978/j.issn.2218-6751.2015.01.11.
[10] L.A. Elliott, G.A. Doherty, K. Sheahan, E.J. Ryan, Human tumor-infiltrating myeloid cells: phenotypic and functional diversity, Front. Immunol. 8 (2017), https://doi.org/10.3389/fimmu.2017.00086.
[11] R. Ostuni, F. Kratochvill, P.J. Murray, G. Natoli, Macrophages and cancer: from mechanisms to therapeutic implications, Trends Immunol. 36 (2015) 229–239, https://doi.org/10.1016/j.it.2015.02.004.
[12] A. Sica, P. Allavena, A. Mantovani, Cancer related inflammation: the macrophage connection, Canc. Lett. 267 (2008) 204–215, https://doi.org/10.1016/j.canlet.2008.03.028.
[13] G. Solinas, G. Germano, A. Mantovani, P. Allavena, Tumor-associated macrophages (TAM) as major players of the cancer-related inflammation, J. Leukoc. Biol. 86 (2009) 1065–1073, https://doi.org/10.1189/jlb.0609385.
[14] R. Noy, J.W. Pollard, Tumor-associated macrophages: from mechanisms to therapy, Immunity 41 (2014) 49–61, https://doi.org/10.1016/j.immuni.2014.06.010.
[15] Y. Mao, N. Eissler, K Le Blanc, et al., Targeting suppressive myeloid cells potentiates checkpoint inhibitors to control spontaneous neuroblastoma, Clin. Canc. Res. 22 (2016) 3849–3859, https://doi.org/10.1158/1078-0432.CCR-15-1912.
[16] S.M. Pyonteck, L. Akkari, A.J. Schuhmacher, et al., CSF-1R inhibition alters macrophage polarization and blocks glioma progression, Nat. Med. 19 (2013) 1264–1272, https://doi.org/10.1038/nm.3337.
[17] C.H. Ries, M.A. Cannarile, S. Hoves, et al., Targeting tumor-associated macrophages with anti-CSF-1R antibody reveals a strategy for cancer therapy, Canc. Cell 25 (2014) 846–859, https://doi.org/10.1016/j.ccr.2014.05.016.
[18] M.F. Cuccarese, J.M. Dubach, C. Pfirschke, et al., Heterogeneity of macrophage infiltration and therapeutic response in lung carcinoma revealed by 3D organ imaging, Nat. Commun. 8 (2017) 14293, https://doi.org/10.1038/ncomms14293.
[19] S.V. Sharma, D.A. Haber, J. Settleman, Cell line-based platforms to evaluate the therapeutic efficacy of candidate anticancer agents, Nat. Rev. Canc. 10 (2010) 241–253, https://doi.org/10.1038/nrc2820.
[20] P. Horvath, N. Aulner, M. Bickle, et al., Screening out irrelevant cell-based models of disease, Nat. Rev. Drug Discov. 15 (2016) 751–769, https://doi.org/10.1038/nrd.2016.175.
[21] C.J. Lovitt, T.B. Shelper, V.M. Avery, Cancer drug discovery: recent innovative approaches to tumor modeling, Expet Opin. Drug Discov. 11 (2016) 885–894, https://doi.org/10.1080/17460441.2016.1214562.
[22] L. Hutchinson, R. Kirk, High drug attrition rates—where are we going wrong? Nat. Rev. Clin. Oncol. 8 (2011) 189–190, https://doi.org/10.1038/nrclinonc.2011.34.
[23] S.J. Turley, V. Cremasco, J.L. Astarita, Immunological hallmarks of stromal cells in the tumour microenvironment, Nat. Rev. Immunol. 15 (2015) 669–682, https://doi.org/10.1038/nri3902.
[24] Z. Liu, B. Delavan, R. Roberts, W. Tong, Lessons Learned from two decades of anticancer drugs, Trends Pharmacol. Sci. 38 (2017) 852–872, https://doi.org/10.1016/j.tips.2017.06.005.
[25] V.E. Santo, M.F. Estrada, S.P. Rebelo, et al., Adaptable stirred-tank culture strategies for large scale production of multicellular spheroid-based tumor cell models, J. Biotechnol. 221 (2016) 118–129, https://doi.org/10.1016/j.jbiotec.2016.01.031.
[26] J.A. Hickman, R. Graeser, R. de Hoogt, et al., Three-dimensional models of cancer for pharmacology and cancer cell biology: capturing tumor complexity in vitro/ex vivo, Biotechnol. J. 9 (2014) 1115–1128, https://doi.org/10.1002/biot.201300492.
[27] L.B. Weiswald, D. Bellet, V. Dangles-Marie, Spherical cancer models in tumor biology, Neoplasia 17 (2015) 1–15, https://doi.org/10.1016/j.neo.2014.12.004.
[28] M.F. Estrada, S.P. Rebelo, E.J. Davies, et al., Modelling the tumour microenvironment in long-term microencapsulated 3D co-cultures recapitulates phenotypic features of disease progression, Biomaterials 78 (2015) 50–61, https://doi.org/10.1016/j.biomaterials.2015.11.030.
[29] J. Kuen, D. Darowski, T. Kluge, M. Majety, Pancreatic cancer cell/fibroblast co-culture induces M2 like macrophages that influence therapeutic response in a 3D model, PLoS One 12 (2017), https://doi.org/10.1371/journal.pone.0182039 e0182039.
[30] N. Linde, C.M. Gutschalk, C. Hoffmann, et al., Integrating macrophages into organotypic co-cultures: a 3D in vitro model to study tumor-associated macrophages, PLoS One 7 (2012), https://doi.org/10.1371/journal.pone.0040058.
[31] D. Martinez-Marin, C. Jarvis, T. Nelius, et al., PEDF increases the tumoricidal activity of macrophages towards prostate cancer cells in vitro, PLoS One 12 (2017), https://doi.org/10.1371/journal.pone.0174968 e0174968.
[32] D. Rama-Esendagli, G. Esendagli, G. Yilmaz, D. Guc, Spheroid formation and invasion capacity are differentially influenced by co-cultures of fibroblast and macrophage cells in breast cancer, Mol. Biol. Rep. 41 (2014) 2885–2892, https://doi.org/10.1007/s11033-014-3144-3.
[33] X. Liu, R. Kiefl, C. Roskopf, et al., Interactions among lung cancer cells, fibroblasts, and macrophages in 3D Co-Cultures and the impact on MMP-1 and VEGF expression, PLoS One 11 (2016), https://doi.org/10.1371/journal.pone.0156268 e0156268.
[34] E.S. Nakasone, H.A. Askautrud, T. Kees, et al., Imaging tumor-stroma interactions during chemotherapy reveals contributions of the microenvironment to resistance, Canc. Cell 21 (2012) 488–503, https://doi.org/10.1016/j.ccr.2012.02.017.
[35] A. Schambach, D. Mueller, M. Galla, et al., Overcoming promoter competition in packaging cells improves production of self-inactivating retroviral vectors, Gene Ther. 13 (2006) 1524–1533, https://doi.org/10.1038/sj.gt.3302807.
[36] S. Haubeiss, J.O. Schmid, T.E. Mürdter, et al., Dasatinib reverses cancer-associated fibroblasts (CAFs) from primary lung carcinomas to a phenotype comparable to that of normal fibroblasts, Mol. Canc. 9 (2010) 168, https://doi.org/10.1186/1476-4598-9-168.
[37] S. Madar, R. Brosh, Y. Buganim, et al., Modulated expression of WFDC1 during carcinogenesis and cellular senescence, Carcinogenesis 30 (2009) 20–27, https://doi.org/10.1093/carcin/bgn232.
[38] A. Rudisch, M.R. Dewhurst, L.G. Horga, et al., High EMT signature score of invasive non-small cell lung cancer (NSCLC) cells correlates with NFκB driven colony-stimulating factor 2 (CSF2/GM–CSF) secretion by neighboring stromal fibroblasts, PLoS One 10 (2015), https://doi.org/10.1371/journal.pone.0124283 e0124283.
[39] K. Stock, M.F. Estrada, S. Vidic, et al., Capturing tumor complexity in vitro: comparative analysis of 2D and 3D tumor models for drug discovery, Sci. Rep. 6 (2016) 28951, https://doi.org/10.1038/srep28951.
[40] E.J. Gualda, H. Pereira, T. Vale, et al., SPIM-fluid: open source light-sheet based platform for high-throughput imaging, Biomed. Optic Express 6 (2015) 4447, https://doi.org/10.1364/BOE.6.004447.
[41] M. Egeblad, M.G. Rasch, V.M. Weaver, Dynamic interplay between the collagen scaffold and tumor evolution, Curr. Opin. Cell Biol. 22 (2010) 697–706, https://doi.org/10.1016/j.ceb.2010.08.015.
[42] S. Gopal, L. Veracini, D. Grall, et al., Fibronectin-guided migration of carcinoma collectives, Nat. Commun. 8 (2017) 14105, https://doi.org/10.1038/ncomms14105.
[43] D.I. Gabrilovich, S. Ostrand-Rosenberg, V. Bronte, Coordinated regulation of myeloid cells by tumours, Nat. Rev. Immunol. 12 (2012) 253–268, https://doi.org/10.1038/nri3175.
[44] V. Kumar, S. Patel, E. Tcyganov, D.I. Gabrilovich, The nature of myeloid-derived suppressor cells in the tumor microenvironment, Trends Immunol. 37 (2016) 208–220, https://doi.org/10.1016/j.it.2016.01.004.
[45] A. Mantovani, F. Marchesi, A. Malesci, et al., Tumour-associated macrophages as treatment targets in oncology, Nat. Rev. Clin. Oncol. (2017), https://doi.org/10.1038/nrclinonc.2016.217.
[46] M. Miyake, S. Hori, Y. Morizawa, et al., CXCL1-Mediated interaction of cancer cells with tumor-associated macrophages and cancer-associated fibroblasts promotes tumor progression in human bladder cancer, Neoplasia 18 (2016) 636–646, https://doi.org/10.1016/j.neo.2016.08.002.
[47] S. Shigdar, Y. Li, S. Bhattacharya, et al., Inflammation and cancer stem cells,

Canc. Lett. 345 (2014) 271–278, https://doi.org/10.1016/j.canlet.2013.07.031.
[48] Q. Guo, Z. Jin, Y. Yuan, et al., New mechanisms of tumor-associated macrophages on promoting tumor progression: recent research advances and potential targets for tumor immunotherapy, J Immunol Res. 2016 (2016) 1–12, https://doi.org/10.1155/2016/9720912.
[49] M. Jaguin, N. Houlbert, O. Fardel, V. Lecureur, Polarization profiles of human M-CSF-generated macrophages and comparison of M1-markers in classically activated macrophages from GM-CSF and M-CSF origin, Cell. Immunol. 281 (2013) 51–61, https://doi.org/10.1016/j.cellimm.2013.01.010.
[50] F.O. Martinez, L. Helming, S. Gordon, Alternative activation of macrophages: an immunologic functional perspective, Annu. Rev. Immunol. 27 (2009) 451–483, https://doi.org/10.1146/annurev.immunol.021908.132532.
[51] A. Chang, Chemotherapy, chemoresistance and the changing treatment landscape for NSCLC, Lung Canc. 71 (2011) 3–10, https://doi.org/10.1016/j.lungcan.2010.08.022.
[52] S. Dasari, P. Bernard Tchounwou, Cisplatin in cancer therapy: molecular mechanisms of action, Eur. J. Pharmacol. 740 (2014) 364–378, https://doi.org/10.1016/j.ejphar.2014.07.025.
[53] D.C. Strachan, B. Ruffell, Y. Oei, et al., CSF1R inhibition delays cervical and mammary tumor growth in murine models by attenuating the turnover of tumor-associated macrophages and enhancing infiltration by CD8 + T cells, OncoImmunology 2 (2013), https://doi.org/10.4161/onci.26968 e26968.
[54] Y. Zhu, B.L. Knolhoff, M.A. Meyer, et al., CSF1/CSF1R blockade reprograms tumor-infiltrating macrophages and improves response to t-cell checkpoint immunotherapy in pancreatic cancer models, Canc. Res. 74 (2014) 5057–5069, https://doi.org/10.1158/0008-5472.CAN-13-3723.
[55] C.L. Chang, Y.T. Hsu, C.C. Wu, et al., Dose-dense chemotherapy improves mechanisms of antitumor immune response, Canc. Res. 73 (2013) 119–127, https://doi.org/10.1158/0008-5472.CAN-12-2225.
[56] A.R. de Biasi, J. Villena-Vargas, P.S. Adusumilli, Cisplatin-induced antitumor immunomodulation: a review of preclinical and clinical evidence, Clin. Canc. Res. 20 (2014) 5384–5391, https://doi.org/10.1158/1078-0432.CCR-14-1298.
[57] L. Prudkin, D.D. Liu, N.C. Ozburn, et al., Epithelial-to-mesenchymal transition in the development and progression of adenocarcinoma and squamous cell carcinoma of the lung, Mod. Pathol. 22 (2009) 668–678, https://doi.org/10.1038/modpathol.2009.19.
[58] G.K. Chimal-Ramírez, N.A. Espinoza-Sánchez, D. Utrera-Barillas, et al., MMP1, MMP9, and COX2 expressions in promonocytes are induced by breast cancer cells and correlate with collagen degradation, transformation-like morphological changes in MCF-10A acini, and tumor aggressiveness, BioMed Res. Int. 2013 (2013) 1–15, https://doi.org/10.1155/2013/279505.
[59] S. Hauptmann, G. Zwadlo-Klarwasser, M. Jansen, et al., Macrophages and multicellular tumor spheroids in co-culture: a three-dimensional model to study tumor-host interactions. Evidence for macrophage-mediated tumor cell proliferation and migration, Am. J. Pathol. 143 (1993) 1406–1415.
[60] A.F. Ochsenbein, P. Klenerman, U. Karrer, et al., Immune surveillance against a solid tumor fails because of immunological ignorance, Immunology 96 (1999) 2233–2238, https://doi.org/10.1073/pnas.96.5.2233.
[61] V. Dangles-Marie, S. Richon, M. El-Behi, et al., A three-dimensional tumor cell defect in activating autologous CTLs is associated with inefficient antigen presentation correlated with heat shock protein-70 down-regulation, Canc. Res. 63 (2003) 3682–3687.
[62] V. Dangles, P. Validire, M. Wertheimer, et al., Impact of human bladder cancer cell architecture on autologous T-lymphocyte activation, Int. J. Canc. 98 (2002) 51–56, https://doi.org/10.1002/ijc.10140.
[63] C. Feder-Mengus, S. Ghosh, W.P. Weber, et al., Multiple mechanisms underlie defective recognition of melanoma cells cultured in three-dimensional architectures by antigen-specific cytotoxic T lymphocytes, Br. J. Canc. 96 (2007) 1072–1082, https://doi.org/10.1038/sj.bjc.6603664.
[64] S. Ghosh, R. Rosenthal, P. Zajac, et al., Culture of melanoma cells in 3-dimensional architectures results in impaired immunorecognition by cytotoxic T lymphocytes specific for Melan-A/MART-1 tumor-associated antigen, Ann. Surg. 242 (2005) 851–857, https://doi.org/10.1097/01.sla.0000189571.84213.b0 discussion 858.
[65] S.A. Almatroodi, C.F. McDonald, I.A. Darby, D.S. Pouniotis, Characterization of m1/m2 tumour-associated macrophages (TAMs) and Th1/Th2 cytokine profiles in patients with NSCLC, Cancer Microenviron 9 (2016) 1–11, https://doi.org/10.1007/s12307-015-0174-x.
[66] Y. Lavin, S. Kobayashi, A. Leader, et al., Innate immune landscape in early lung adenocarcinoma by paired single-cell analyses, Cell 169 (2017) 750–765, https://doi.org/10.1016/j.cell.2017.04.014 e17.
[67] T. Silzle, M. Kreutz, M.A. Dobler, et al., Tumor-associated fibroblasts recruit blood monocytes into tumor tissue, Eur. J. Immunol. 33 (2003) 1311–1320, https://doi.org/10.1002/eji.200323057.
[68] G. Comito, E. Giannoni, C.P. Segura, et al., Cancer-associated fibroblasts and M2-polarized macrophages synergize during prostate carcinoma progression, Oncogene 33 (2014) 2423–2431, https://doi.org/10.1038/onc.2013.191.
[69] M. Ksiazkiewicz, E. Gottfried, M. Kreutz, et al., Importance of CCL2-CCR2A/2B signaling for monocyte migration into spheroids of breast cancer-derived fibroblasts, Immunobiology 215 (2010) 737–747, https://doi.org/10.1016/j.imbio.2010.05.019.
[70] H.H. Popper, Progression and metastasis of lung cancer, Canc. Metastasis Rev. 35 (2016) 75–91, https://doi.org/10.1007/s10555-016-9618-0.
[71] J.M. Walker, Tumor Immunology, Springer New York, New York, NY, 2016.
[72] R. Wang, J. Zhang, S. Chen, et al., Tumor-associated macrophages provide a suitable microenvironment for non-small lung cancer invasion and progression, Lung Canc. 74 (2011) 188–196, https://doi.org/10.1016/j.lungcan.2011.04.009.
[73] M.S. Macauley, P.R. Crocker, J.C. Paulson, Siglec-mediated regulation of immune cell function in disease, Nat. Rev. Immunol. 14 (2014) 653–666, https://doi.org/10.1038/nri3737.
[74] S.P. Méndez-Huergo, A.G. Blidner, G.A. Rabinovich, Galectins: emerging regulatory checkpoints linking tumor immunity and angiogenesis, Curr. Opin. Immunol. 45 (2017) 8–15, https://doi.org/10.1016/j.coi.2016.12.003.
[75] R. Beatson, V. Tajadura-Ortega, D. Achkova, et al., The mucin MUC1 modulates the tumor immunological microenvironment through engagement of the lectin Siglec-9, Nat. Immunol. 17 (2016) 1273–1281, https://doi.org/10.1038/ni.3552.
[76] R. Takamiya, K. Ohtsubo, S. Takamatsu, et al., The interaction between Siglec-15 and tumor-associated sialyl-Tn antigen enhances TGF-?? secretion from monocytes/macrophages through the DAP12-Syk pathway, Glycobiology 23 (2013) 178–187, https://doi.org/10.1093/glycob/cws139.
[77] D.A. Fennell, Y. Summers, J. Cadranel, et al., Cisplatin in the modern era: the backbone of first-line chemotherapy for non-small cell lung cancer, Canc. Treat Rev. 44 (2016) 42–50, https://doi.org/10.1016/j.ctrv.2016.01.003.
[78] A.E. Prota, K. Bargsten, D. Zurwerra, et al., Molecular mechanism of action of microtubule-stabilizing anticancer agents, Science 80 (339) (2013) 587–590, https://doi.org/10.1126/science.1230582.
[79] F. Klemm, J.A. Joyce, Microenvironmental regulation of therapeutic response in cancer, Trends Cell Biol. 25 (2015) 198–213, https://doi.org/10.1016/j.tcb.2014.11.006.
[80] R.A. Singh, A. Sodhi, Antigen presentation by cisplatin-activated macrophages: role of soluble factor(s) and second messengers, Immunol. Cell Biol. 76 (1998) 513–519, https://doi.org/10.1046/j.1440-1711.1998.00769.x.
[81] A. Sodhi, Mechanism of NF-κB translocation in macrophages treated in vitro with cisplatin, Immunol. Lett. 63 (1998) 9–17, https://doi.org/10.1016/S0165-2478(98)00043-1.
[82] Z.G. Fridlender, J. Sun, S. Singhal, et al., Chemotherapy delivered after viral immunogene therapy augments antitumor efficacy via multiple immune-mediated mechanisms, Mol. Ther. 18 (2010) 1947–1959, https://doi.org/10.1038/mt.2010.159.
[83] L. Bracci, G. Schiavoni, A. Sistigu, F. Belardelli, Immune-based mechanisms of cytotoxic chemotherapy: implications for the design of novel and rationale-based combined treatments against cancer, Cell Death Differ. 21 (2014) 15–25, https://doi.org/10.1038/cdd.2013.67.
[84] S. Park, S. Kang, X. Chen, et al., Tumor suppression via paclitaxel-loaded drug carriers that target inflammation marker upregulated in tumor vasculature and macrophages, Biomaterials 34 (2013) 598–605, https://doi.org/10.1016/j.biomaterials.2012.10.004.
[85] A. Javeed, M. Ashraf, A. Riaz, et al., Paclitaxel and immune system, Eur. J. Pharmaceut. Sci. 38 (2009) 283–290, https://doi.org/10.1016/j.ejps.2009.08.009.
[86] D. Laoui, E. van Overmeire, P. de Baetselier, et al., Functional relationship between tumor-associated macrophages and macrophage colony-stimulating factor as contributors to cancer progression, Front. Immunol. 5 (2014) 1–15, https://doi.org/10.3389/fimmu.2014.00489.
[87] C. Ngambenjawong, H.H. Gustafson, S.H. Pun, Progress in tumor-associated macrophage (TAM)-targeted therapeutics, Adv. Drug Deliv. Rev. (2017), https://doi.org/10.1016/j.addr.2017.04.010.
[88] Y. Mao, I. Poschke, R. Kiessling, Tumour-induced immune suppression: role of inflammatory mediators released by myelomonocytic cells (Review), J. Intern. Med. 276 (2014) 154–170.